Luttinger-liquid state of the zigzag double chain

T. F. A. Müller and T. M. Rice
Institut für Theoretische Physik, ETH-Hönggerberg, CH-8093 Zurich, Switzerland
(Received 21 August 1998)

The zigzag double chain is investigated using Lanczos techniques. The weak-coupling limit is similar to that of a ladder system which is known to have a spin gap at half-filling at all coupling strengths. But the half-filled zigzag system is gapless at strong coupling. The question whether a spin gap occurs upon doping is investigated. It is shown that the doped zigzag chain is a Luttinger liquid in which the holes repel each other. The criterion is based on exact diagonalization techniques for open shell boundary conditions. As a further corroboration, the hole-hole and the hole-spin correlations are also computed. [S0163-1829(99)07427-5]

I. INTRODUCTION

The study of low-dimensional quantum magnets and the effects of doping is a major topic at present, stimulated by the discovery of high-T_c superconductivity in the planar cuprates.[1] The wide range of possible cuprate structures has also encouraged the study of one-dimensional (1D) systems and those which are intermediate between one and two dimensions (2D).[2] One such system comes through assembling chains together to form simple ladders and recent studies have focused on the very interesting phase diagrams that result.[3,4] However, cuprates chains may be assembled in another way, namely to form a zigzag double chain.

Recent measurements performed on the underdoped compound $YBa_2Cu_4O_8$ ($T_c \simeq 80$) have shown that for $T < 200$ K the *c*-axis dc conductivity is *metallic*, implying the onset of coherent three-dimensional (3D) conductivity[5] just above T_c. This difference with other underdoped superconductors is explained by the special structure of this compound. It forms a stack of planes where layers of zigzag Cu-O double-chain sandwich bilayers of CuO_2 square planes. Recent measurements[6] have established that the double-chain layers only were responsible for the coherent *c*-axis transport. The 3D coupling between the double chains arises through virtual hopping processes, involving empty states in the CuO_2 square planes. However, the effective hopping matrix elements between the double chains are very small. In fact, band-structure calculations display only a small dispersion along the *c* axis [$\Delta E \simeq 0.05$ eV (Ref. 7)] and an estimate of the perpendicular interchain coherent hopping from magnetoresistance experiments gives a value of $t_c \simeq 3$ meV.[6]

Moreover, the double-chain resistivity shows a standard Landau form $\rho_{\text{chain}} = \rho_0 + AT^2$ for $T < 450$ K,[5] with $\rho_0 = 0.5\ \mu\Omega$ cm and $A = 1.47$ nΩ cm/K^2. The low value of ρ_0 confirms the very high level of perfection of the double chains. Previous nuclear magenetic resonance (NMR) measurements showed the existence of a Korringa law in $1/(T_1T)$ for the copper in the double chains.[8,9] These results suggest that the double chains form a 3D Landau-Fermi liquid although the coupling between double chains is very weak when compared to intrachain couplings. Note that in the compound $YBa_2Cu_4O_8$ the double chains are self-doped with a hole concentration $\delta \simeq 0.3$–0.35. This system is therefore a very good example of a doped quasi-1D cuprate. Further replacing Y by Pr should make the planes insulating and allow the study of the weakly coupled and doped double chains down to low temperatures.

In the noninteracting limit, a double chain is described by two bands (bonding and antibonding). The glide symmetry of the system leads to a degeneracy at $k = \pi$ in the double-band description, so these bands are reminiscent of the one-band system of the 1D chain with longer-range hopping. Thus, near half-filling the Fermi surface is given by four points as in the case of the simple two-leg ladder. The weak-coupling limit of the Hubbard model for this system, examined by Fabrizio,[10] Balents and Fisher,[11] renormalizes to a strong-coupling fixed point with a spin gap, physically related to the formation of hole pairs.

This contrasts with theoretical studies of the half-filled double chain in the strong-coupling regime[12] which show that a weak ferromagnetic interchain coupling leads to a gapless phase. A small antiferromagnetic interchain coupling opens only an exponentially small gap. The key question whether or not this gapless phase evolves into a gapped phase upon doping will be investigated in this paper, using exact diagonalization techniques with parameter values appropriate to the cuprates.

Along the chain, the copper spins are coupled by the 180° Cu-O-Cu interaction, leading to a strong antiferromagnetic interaction (J_2) as in the ladder geometry. The interchain magnetic coupling J_1 arises from a 90° Cu-O-Cu bond and is thus expected to be ferromagnetic with a much smaller magnitude than J_2, $|J_1|/J_2 \simeq 0.1$–0.2.[13] Moreover, the zigzag coupling introduces frustration in the spin ordering. Experimental estimates of the magnetic coupling on the stoichiometric single-chain (double-chain) compound Sr_2CuO_3 ($SrCuO_2$) give similar values, $J_2 \simeq 1800$–2100 K.[14,15] The magnetic coupling is comparable with the value $J_2 \simeq 1500$ K,[16] found in the ladder compound $(SrCa)_{14}Cu_{24}O_{41}$. The magnetic coupling in $YBa_2Cu_4O_s$ is also expected to have approximately similar values. In the following, the value $J_2 = 170$ meV ($\simeq 2000$ K) will be used. The interchain coupling is arbitrarily chosen to be $J_1 = -20$ meV.

Upon doping, hopping processes are allowed. The values estimated for $(SrCa)_{14}Cu_{24}O_{41}$ (Ref. 17) will be used where a similar structural unit separates the two-leg ladders in the

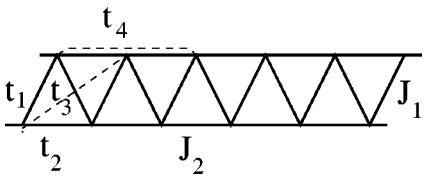

FIG. 1. The effective model for the CuO_2 double chain used in this paper.

ladder planes. A detailed study of the band structure showed that sizable longer-range hopping matrix elements occur in a double chain. The matrix element convention is displayed in Fig. 1 with values of $t_1=0.018$ eV, $t_2=0.537$ eV, $t_3=0.053$ eV, and $t_4=0.106$ eV predicted from local-density approximation (LDA) calculations.

II. WEAK-COUPLING

We begin with a recapitulation of the results in the weak-coupling limit which is closely related to the analyses of Fabrizio[10] and Balents and Fisher[11] for models with two bands at the Fermi energy. At half-filling, the Fermi velocities of the bonding and antibonding bands are taken to be equal. First it is checked if the fixed point at half-filling (called C0S0 in Ref. 11) is robust for different Fermi velocities, characteristic of the double-chain energy bands. The couplings constants are defined in Fig. 2 and follow the g-ology notation.[18,19] The g_1 processes denote the backscatterings implying only one or both bands, g_2 denotes the forward scatterings between left and right movers, whereas g_4 stands for forward scattering between right (or left) movers. In the one-loop expansion the g_4 couplings will not lead to any divergent diagram and are independent of all the others couplings.[18] They will not be considered any further. g_3 denotes the Umklapp processes occurring at half-filling when the Fermi energy cut both bands, with $k_{\mathrm{F,a}}+k_{\mathrm{F,b}}=\pi$.

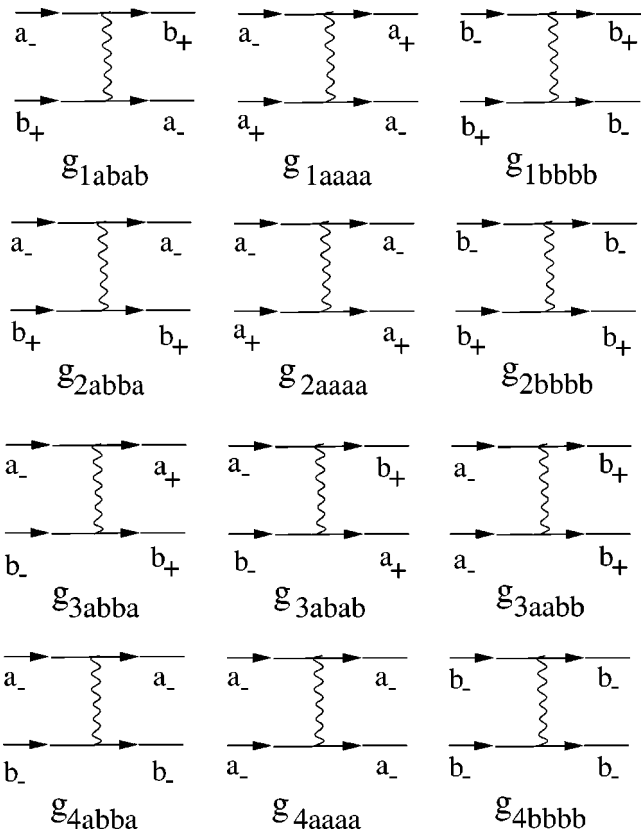

FIG. 2. The different couplings for a four-point Fermi surface. Each one is illustrated with one possible scattering process.

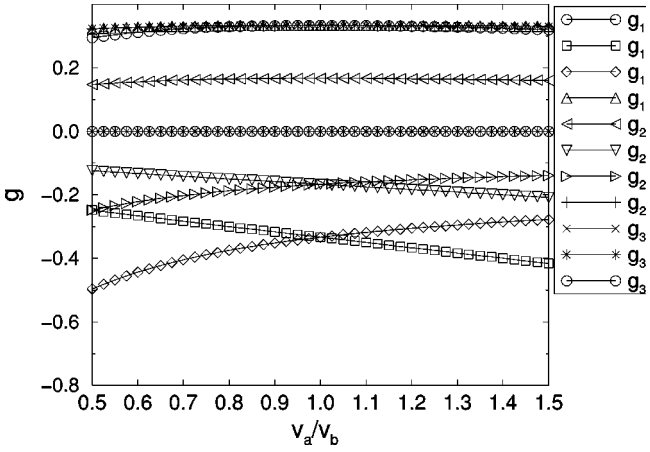

FIG. 3. The coupling coefficients g_{i0} for different velocity ratios at half-filling.

The renormalization group (RG) flows are derived according to the standard methods described in the literature.[18] The differential equations for the couplings in the case with all Umklapp processes of Fig. 2 and different Fermi velocities are given in the appendix.

At half-filling, the three couplings $g_{3aabb}, g_{3abab}, g_{3abba}$ are allowed, leading to a system of 11 coupled differential equations. The flow of equations are integrated numerically up to the first divergence Λ where all couplings are assumed to diverge like

$$g_i=\frac{\Lambda g_{i,0}}{1-\Lambda l}.$$

The coefficient $g_{i,0}$ is then computed. In Fig. 3, the coefficients $g_{i,0}$ are plotted as a function of the Fermi speed ratio v_a/v_b, where v_a (v_b) is the Fermi energy at $k_{\mathrm{F,a}}$ ($k_{\mathrm{F,b}}$). It is seen that no qualitative change occurs around $\alpha/\beta=1$. For the band parameters given above, the ratio of the velocities is $v_a/v_b\simeq 1.08$ and the same phase as for $\alpha=\beta$, (i.e., a C0S0) occurs in agreement with earlier studies.[10,11] Thus, this is clearly in contradiction with the experimental and analytical study of the half-filled double-chain system.[14,12] The introduction of strong interactions will change the nature of the fixed point.

III. STRONG-COUPLING LIMIT

The strong-interaction limit is studied in the framework of the t-J model with the Hamiltonian

$$H=-\sum_{\langle i,j\rangle,\sigma}(t_{ij}\tilde{c}^{\dagger}_{i,\sigma}\tilde{c}_{j,\sigma}+\mathrm{H.c.})+J_2\sum_i\left(\mathbf{S}_i\mathbf{S}_{i+e_x}-\frac{1}{4}n_in_{i+e_x}\right)+J_1\sum_{\langle i,i'\rangle}\mathbf{S}_i\mathbf{S}_{i'},\quad(1)$$

where the last sum $\Sigma_{\langle i,i'\rangle}$ is taken over all the interchain bonds. J_1 is chosen to be negative in order to account for the ferromagnetic interaction. The projection onto singly occupied sites is included in the operator $\tilde{c}_{j,\sigma}=c_{j,\sigma}(1-n_{j,-\sigma})$.

As pointed out above, this system is equivalent to a single chain, however, the notation will follow the double-chain representation. In the one-electron picture, the two bands can be discriminated by using the label $\sigma_r=+(-)$ denoting the bonding (antibonding) band such that the energy $\epsilon_{\sigma_r}(k)$ fulfills the relationship $\epsilon_+(k_z)=\epsilon_-(2\pi-k_z)$. This relationship is a consequence of the glide symmetry of the system. Two analogous parameters $\{k_z,\sigma_r\}$ will be used to label the many-body wave function (where k_z is now the total wave vector and σ_r the eigenvalue under exchange of the chains). In the subspace $S_z=0$, the symmetry due to the rotation by 180° of all spins (all spins flipped) is also used. It can be labeled by the character of the rotation $\sigma_s=\pm 1$. This splits the Hilbert space into one with even total spin, $S=2n$ $(\sigma_s=+1)$, and one with odd total spin, $S=2n+1$ $(\sigma_s=-1)$. In general, the lowest state in the corresponding subspace has the minimal total spin, i.e., is a singlet (triplet) for $\sigma_s=+1$ (-1). The different results will be plotted as a function of $\{k_z,\sigma_r,\sigma_s\}$.

A. Open shell and Luttinger liquid

Usually, in order to avoid overestimating the possibility of a pairing instability, closed shell boundary conditions are used.[20] Here, open shell boundary conditions (OSBC) with an even number of holes will be investigated. In the noninteracting limit, these BC's allow partially filled band levels at $k=k_F$ such that ground-state energy is degenerate, implying two states, one with the total wave function $k=0$ and one with $k=2k_F$. In the strong-coupling limit, a Luttinger liquid (LL) with hole repulsion will favor the $k=2k_F$ ground state since then the two holes have the same wave vector $k=k_F$, minimizing their repulsion. In order to illustrate this effect the 1D t-J model with only nearest-neighbor interactions will be considered. It is well-known that with hole doping, this 1D system is a Luttinger liquid.[21–23] Therefore, in this case, finite-size effects occurring for small systems can be studied.

In the upper (lower) panel of Fig. 4 the energy spectrum as a function of k is plotted for a 10 (20)-site chain doped with two holes, using periodic (antiperiodic) boundary conditions, (PBC) (APBC). In the subspace $\sigma_s=1$, the lowest energy is at $2k_F=4\pi/5$ as expected for a LL. However, the ground state of this system is a triplet in the subspace $\sigma_s=-1$ at $k=0$. This is interpreted as a finite-size effect due to the small size of the cluster and it is reminiscent of the singlet-triplet degeneracy of a LL. This can be better understood when considering the larger cluster with 20 sites. There, the ground state is at $2k_F=9\pi/10$ with $\sigma_s=1$, slightly below the triplet state at $k=0$.

B. Double chain

The study of the double-chain system will be based on a 2×10 cluster with a doping $n_h=2$ and $n_h=6$ holes. The case with $n_h=2$ is first considered in order to investigate the behavior of the 2 holes introduced in the system. It is of interest

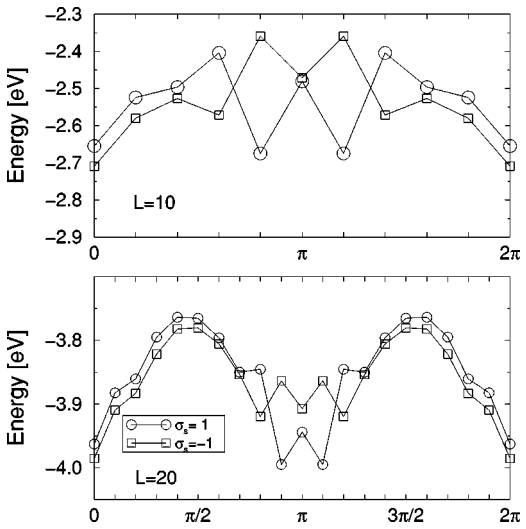

FIG. 4. The total-energy spectrum for a single chain doped with two holes. The uppermost panel displays the values for a 10-site chain using PBC. The lowermost panel displays the values for a 20-site chain using APBC.

to see if they form pairs leading to a spin gap, as in the simple ladder or if they repel each other favoring a LL. Contrary to the 1D case discussed above, if the 2 holes repel each other, it will introduce a supplementary frustration in the antiferromagnetic order of the spins in the chains. For such a small system this effect can be important. It will be seen, however, that the qualitative picture described above for the single chain is not strongly modified. The case with $n_h=6$ is also discussed since it is the closest to the compound $YBa_2Cu_4O_8$ that has self-doped double chains with $\delta\simeq 0.3$–0.35.

In Fig. 5, the lowest eigenvalues of a 2×10 cluster with 2(6) holes is plotted as a function of k for PBC(APBC). Both PBC and APBC lead to OSBC in both cases. The system doped with 2 holes gives a smaller energy when APBC's are used than when PBC's are used. However, the corresponding Fermi vector is $k_F=\pi/2$, allowing the occurrence of unwanted Umklapp processes. In order to prevent this small-size artifact, PBC's are chosen. In the case

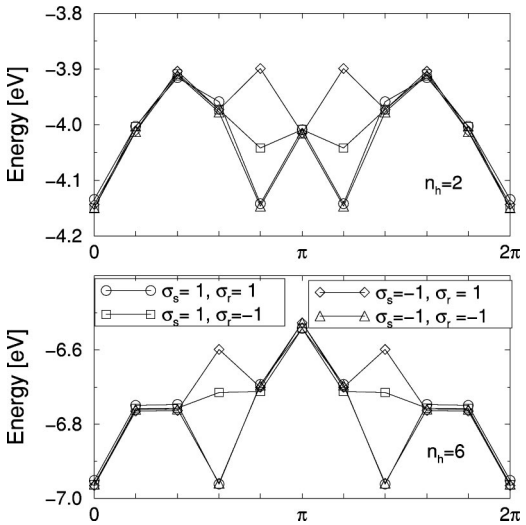

FIG. 5. The upper- (lower-) most panel displays the total-energy spectrum for a 2×10 cluster with 2 (6) holes using PBC (APBC).

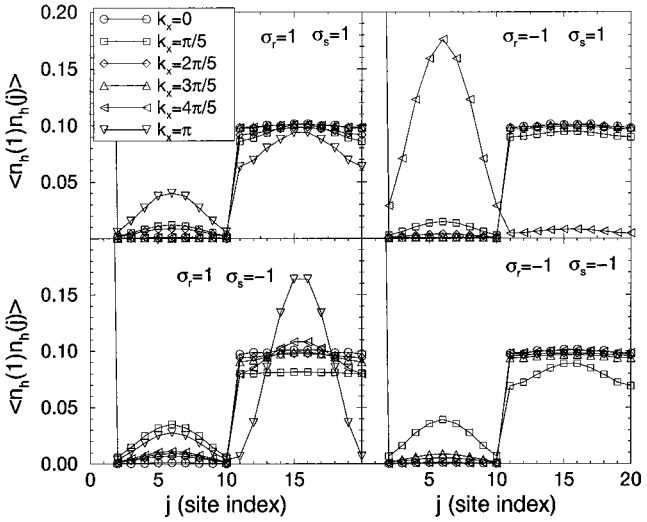

FIG. 6. The hole-hole correlation for a 2×10 cluster with 2 holes using PBC. They are normalized such that $\langle n_h(1)n_h(1)=1$ (this point is out of the graphs). The site index j is chosen such that $1\leqslant j\leqslant10$ labels the sites of the first chain and $11\leqslant j\leqslant20$ labels the sites of the second chain.

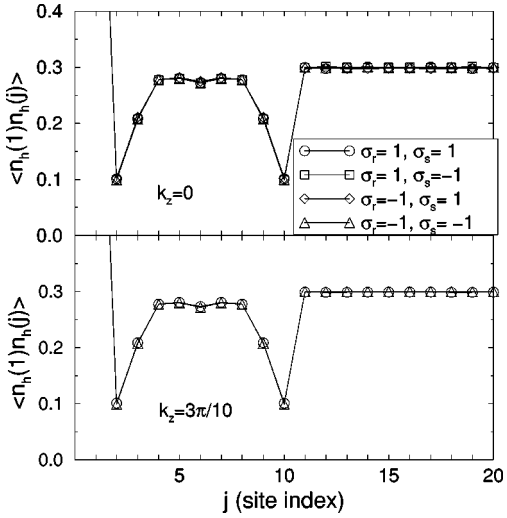

FIG. 7. The hole-hole correlation for a 2×10 cluster with 6 holes using APBC. They are normalized such that $\langle n_h(1)n_h(1)\rangle=1$ (this point is out of the graphs). The site index j is chosen such that $1\leqslant j\leqslant10$ labels the sites of the first chain and $11\leqslant j\leqslant20$ labels the sites of the second chain.

with 6 holes, APBC leads to the OS with the lowest ground state and will be used. In each graph, the four curves give the energies in the subspaces labeled by $\{\sigma_r,\sigma_s\}$. The most striking feature is that the energy curve in the subspace $\{\sigma_r=1,\sigma_s=1\}$ is analogous to the 1D case. It has a local minimum at $2k_F=4\pi/5(3\pi/5)$ for $n_h=2(6)$, indicating that the system is a LL. The lower energy found in the sector $\sigma_s=-1$, we ascribe to a finite-size effect as in the 1D case.

C. Hole-hole correlations

The pairing of holes, if it occurs, can be directly observed in the hole-hole correlation $\langle n_h(1)n_h(j)\rangle$. In Fig. 6 they are plotted in the different subspaces for the $n_h=2$ case. They are normalized such that $\langle n_h(1)n_h(1)\rangle=1$ (this point is not shown in the graphs). The subspace with $\sigma_r=-1,k=\pi$ is equivalent to that with $\sigma_r=1,k=\pi$, and thus only five correlations are plotted in the corresponding subspaces. On the horizontal axis, the site index j is chosen such that $1\leqslant j\leqslant10$ labels the sites of the first chain and $11\leqslant j\leqslant20$ labels the sites of the second chain.

The correlations corresponding to the lowest energies are of interest here since they characterize the ground-state properties. When the first hole is fixed at $j=1$, the second hole has nearly no probability of being on the same chain and is equally found on the sites of the next chain. This shows that the holes repel each other where no correlation is found between the chains and thus that both chains behave independently, forming a LL. A few correlations are peculiar as in the case $\sigma_r=-1,\sigma_s=1,k=4\pi/5$, where both holes are on the same chain but still repel each other. This state has a much higher energy than the ground-state energy and represents an excitation of the system. This point does not modify the proposed picture and will not be discussed further.

In Fig. 7 the hole-hole correlation for a system with six holes is shown. In order to reduce the computing time, only the correlations for $k=0$ and $k=3\pi/5$ corresponding to the lowest energies have been computed. They also show a repulsive correlation. When the first hole is fixed to the first site, the correlation for $j\leqslant10$ displays two spread-out local maxima at $j=4,5$ and $j=7,8$ with a tiny local minimum at $j=6$. This favors the picture of three repulsive holes on the first chain. The branch with $j>10$ is nearly flat again indicating the lack of correlation between the chains. Therefore, the same repulsive character exists for the holes as in the previous case and it is again concluded that this system behaves like a LL.

D. Hole-spin correlation

A property of a LL is the relationship between the spin excitations (spinons) and the holes (holons). The magnetic energy introduces a weak attraction between spinons and holons and just a small energy is necessary to separate these particles allowing them to move freely and independently of each other (spin-charge separation). The $S=1$ ($S_z=1$) manifold of a 2×10 double chain, doped with 2 holes, consists of 2 spinons (each one identified with a $\uparrow\uparrow$-spin pair) and 2 holons as schematically plotted in Fig. 8. The corresponding lowest energies in this subspace are those labeled with $\sigma_s=-1$ (triplets) in Fig. 5.

The correlation between the spins and the holes $A_{ns}(j)=\langle n_h(1)S^z(j)\rangle$ is computed. It is interpreted as fixing one hole at $j=1$ and looking at the remaining spins. In Fig. 9 these hole-spin correlations for the 2×10 cluster doped with two holes in the sectors $k=0$ and $k=4\pi/5$ are plotted. The curves corresponding to the lowest energy states are consistent with each other. For $1\leqslant j\leqslant10$ the correlations show an

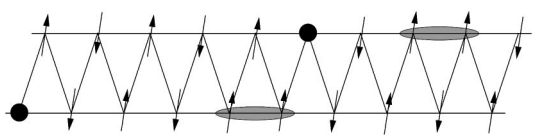

FIG. 8. Schematic plot of 2 spinons and 2 holons in the double-chain system.

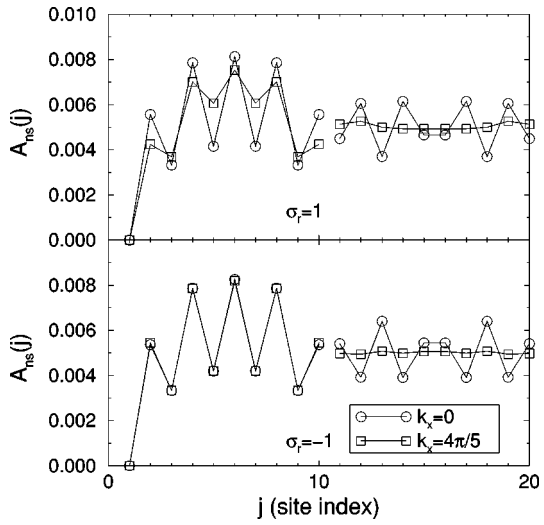

FIG. 9. The hole-spin correlation for a 2×10 cluster with 2 holes and a total magnetization $S_z=1$ using PBC. The site index j is chosen such that $1\leqslant j\leqslant 10$ labels the sites of the first chain and $11\leqslant j\leqslant 20$ labels the sites of the second chain.

alternating function of local maximum and minimum. This means that when one hole is fixed on the first site, the supplementary spins are spread out along the chain (spin-charge separation) with a slight preference for the up spins lying around the hole, reminiscent of the weak spinon-holon attraction. The spins are ordered antiferromagnetically, implying a field felt by the spins of the second chain and thus a relative ordering of the spins at $11\leqslant j\leqslant 20$. This interchain correlation is much less important than the intrachain correlation. It should be pointed out that the hole-hole correlation is the same as in Fig. 7 in the subspace $\sigma_s=-1$, where it was found that holes repel each other, corroborating the LL picture for the doped double chain.

IV. CONCLUSION

Therefore, the strong-coupling limit of the double-chain system displays a completely different behavior than that of the weak-coupling model. In fact the numerical data show strong evidences for a system of decoupled chains, each behaving as a LL without a spin gap. This is consistent with an analogous work using a 1D Hubbard model ($t-t'-U$) but with a positive next nearest hopping.[24] Thus, the fixed point governing the physics of an isolated double chain has been shown to be a LL without hole-pair formation. If hole pairs were formed as in the two-leg ladder, then weak 3D coupling should lead to a superconducting or a charge-density-wave ground state.[25] Instead, a model of weakly coupled Luttinger liquids is found for the double chains in $YBa_2Cu_4O_8$ and from experiment it seems they form a 3D Landau-Fermi liquid.

ACKNOWLEDGMENTS

We wish to thank N. Furukawa for helpful and fruitful discussion. This work was supported by the ''Fond National Suisse.'' Calculations have been performed on the IBM RS/6000-590 and on the DEC AXP 8400 of ETH-Zürich.

TABLE I. Correspondence with the notation of Ref. 11.

g_{1aaaa}	$g_{1\sigma}/2$
g_{1bbbb}	$g_{2\sigma}/2$
g_{1abab}	$g_{x\sigma}/2$
g_{1aabb}	$g_{t\sigma}/2$
g_{2aaaa}	$g_{1\sigma}/4-g_{1\rho}$
g_{2bbbb}	$g_{2\sigma}/4-g_{2\rho}$
g_{2abba}	$g_{x\sigma}/4-g_{x\rho}$
g_{2aabb}	$g_{t\sigma}/4-g_{t\rho}$
g_{3aabb}	$-g_{xu}$
g_{3abba}	$-g_{tu_1}$
g_{3abab}	g_{tu_2}

APPENDIX: RG EQUATIONS

The derivative of the coupling can be written using $\dot{g}=dg/dl$, with $l=-\ln x/(\pi\bar{v})$. $\bar{v}=\frac{1}{2}(v_a+v_b)$ is the average of the Fermi velocities of the antibonding and bonding bands. $x=\omega/E_0$ is the scaling parameter of the system, where E_0 is the cutoff. Thus, the flow is parametrized with $l:0\rightarrow\infty$. Using the parameter $\alpha=\bar{v}/v_a$ and $\beta=\bar{v}/v_b$, the Lie equations for the RG flows of the different couplings are given by

$$\dot{g}_{1abab}=-[g_{1abab}^2+g_{1aabb}^2+g_{3abab}^2-g_{1aabb}g_{2aabb}-g_{3abab}g_{3abba}],$$

$$\dot{g}_{1aaaa}=-[g_{1aaaa}^2\alpha+(g_{3abba}^2+g_{1aabb}g_{2aabb}-g_{3abba}g_{3abab})\beta],$$

$$\dot{g}_{1bbbb}=-[g_{1bbbb}^2\beta+(g_{3abba}^2+g_{1aabb}g_{2aabb}-g_{3abba}g_{3abab})\alpha],$$

$$\dot{g}_{1aabb}=-[\tfrac{1}{2}(g_{1aaaa}g_{2aabb}+g_{1aabb}g_{2aaaa})\alpha+\tfrac{1}{2}(g_{1bbbb}g_{2aabb}+g_{1aabb}g_{2bbbb})\beta+2g_{1abab}g_{1aabb}+g_{3abab}g_{3aabb}-g_{1abab}g_{2aabb}-g_{1aabb}g_{2abba}-g_{3aabb}g_{3abba}],$$

$$\dot{g}_{2abba}=-\tfrac{1}{2}(g_{1abab}^2-g_{2aabb}^2-g_{3abba}^2-g_{3aabb}^2),$$

$$\dot{g}_{2aaaa}=-\tfrac{1}{2}[(g_{1aaaa}^2)\alpha+(g_{1aabb}^2+g_{2aabb}^2-g_{3abab}^2)\beta],$$

$$\dot{g}_{2bbbb}=-\tfrac{1}{2}[(g_{1bbbb}^2)\beta+(g_{1aabb}^2+g_{2aabb}^2-g_{3abab}^2)\alpha]$$

$$\dot{g}_{2aabb}=-[\tfrac{1}{2}(g_{1aabb}g_{1aaaa}+g_{2aabb}g_{2aaaa})\alpha+\tfrac{1}{2}(g_{1aabb}g_{1bbbb}+g_{2aabb}g_{2bbbb})\beta-(g_{2abba}g_{2aabb}+g_{3abba}g_{3aabb})],$$

$$\dot{g}_{3abba} = -[\tfrac{1}{2}(2g_{1aaaa}g_{3abba} - g_{1aaaa}g_{3abab} - g_{3abba}g_{2aaaa})\alpha + \tfrac{1}{2}(2g_{1bbbb}g_{3abba} - g_{1bbbb}g_{3abab} - g_{3abba}g_{2bbbb})\beta - (g_{2abba}g_{3abba} + g_{2aabb}g_{3aabb})],$$

$$\dot{g}_{3abab} = -[-\tfrac{1}{2}g_{2aaaa}g_{3abab}\alpha - \tfrac{1}{2}g_{2bbbb}g_{3abab}\beta + 2g_{1abab}g_{3abab} + g_{1aabb}g_{3aabb} - g_{1abab}g_{3abba} - g_{3abab}g_{2abba} - g_{3aabb}g_{2aabb}],$$

$$\dot{g}_{3aabb} = -[g_{1abab}g_{3aabb} + 2g_{3abab}g_{1aabb} - g_{1aabb}g_{3abba} - g_{3abab}g_{2aabb} - 2g_{3aabb}g_{2abba} - g_{2aabb}g_{3abba}].$$

The meaning of the different couplings is schematically given in Fig. 2. Their notations follow the standard *g*-ology notation and their derivation is analogous to the 1D case.[18] In order to get a direct rewriting of these formulas in terms of the current-algebra notation used by Balents and Fisher, the relationship between the two notations is given in Table I.

[1] J.G. Bednorz and K.A. Müller, Z. Phys. B **64**, 189 (1986).
[2] E. Dagotto and T.M. Rice, Science **271**, 618 (1996).
[3] T.F.A. Müller and T.M. Rice, Phys. Rev. B **58**, 3425 (1998).
[4] C.A. Hayward and D. Poilblanc, Phys. Rev. B **53**, 11 721 (1996).
[5] N.E. Hussey, K. Nozawa, H. Takagi, S. Adachi, and K. Tanabe, Phys. Rev. B **56**, R11 423 (1997).
[6] N.E. Hussey, M. Kibune, H. Nagakawa, N. Miura, Y. Iye, H. Takagi, S. Adachi, and K. Tanabe, Phys. Rev. Lett. **80**, 2909 (1998).
[7] J. Yu, K.T. Park, and A.J. Freeman, J. Phys. C **172**, 467 (1991).
[8] H. Zimmermann, M. Mali, D. Brinkmann, J. Karpinski, E. Kaldis, and S. Rusiecki, Physica C **159**, 681 (1989).
[9] H. Zimmermann, M. Mali, I. Mangelschots, J. Roos, L. Pauli, D. Brinkmann, J. Karpinski, S. Rusiecki, and E. Kaldis, J. Less-Common Met. **164-165**, 138 (1990).
[10] M. Fabrizio, Phys. Rev. B **48**, 15 838 (1993).
[11] L. Balents and M.P.A. Fisher, Phys. Rev. B **53**, 12 133 (1996).
[12] S.R. White and I. Affleck, Phys. Rev. B **54**, 9862 (1996).
[13] T.M. Rice, S. Gopalan, and M. Sigrist, Europhys. Lett. **23**, 445 (1993).
[14] N. Motoyama, H. Eisaki, and S. Uchida, Phys. Rev. Lett. **76**, 3212 (1996).
[15] M. Matsuda, K. Katsumata, K.M. Kojima, M. Larkin, G.M. Luke, J. Merrin, B. Nachumi, Y.J. Uemura, H. Eisaki, N. Motoyama, S. Uchida, and G. Shirane, Phys. Rev. B **55**, R11 953 (1997).
[16] R. S. Eccleston, M. Uehara, J. Akimitsu, H. Eisaki, M. Motoyama, and S. Uchida, Phys. Rev. Lett. **81**, 1702 (1998).
[17] T.F.A. Müller, V. Anisimov, T.M. Rice, I. Dasgupta, and T. Saha-Dasgupta, Phys. Rev. B **57**, R12 655 (1998).
[18] J. Sólyom, Adv. Phys. **28**, 201 (1978).
[19] Only one scattering process per coupling is plotted. However, it should be clear that the other scattering processes are also implied. For instance, g_{1abab} is shown with the process $a_- \to b_+$, $b_+ \to a_-$ but also denotes the process $a_+ \to b_-$, $b_- \to a_+$.
[20] M. Troyer, Ph.D. thesis, ETH-Zürich, 1994.
[21] M. Luchini, M. Ogata, W. Putikka, and T.M. Rice, J. Phys. C **185-189**, 141 (1991).
[22] M. Ogata, M.U. Luchini, S. Sorella, and F.F. Assaad, Phys. Rev. B **66**, 2388 (1991).
[23] H. Shiba and M. Ogata, Prog. Theor. Phys. **108**, 265 (1992).
[24] R. Arita, K. Kuroki, and H. Aoki, Phys. Rev. B **57**, 10 324 (1998).
[25] H. Tsunetsugu, M. Troyer, and T.M. Rice, Phys. Rev. B **51**, 16 456 (1995).